Fluorescent taxoids

RK Guy[1], ZA Scott[2], RD Sloboda[2] and KC Nicolaou[1]

Background: Taxol* is a natural product produced by the Pacific Yew, *Taxus brevifolia*, that has emerged as a prominent chemotherapeutic agent for the treatment of solid tumors. Taxol's biochemical mode of action has been well studied: it binds to microtubules, stabilizing them and preventing their depolymerization to tubulin subunits. At lower dosage levels, taxol also interferes with the normal dynamics of the tubulin–microtubule equilibrium. This biochemical effect causes taxol's ultimate physiological effect, cell cycle arrest; taxol is thought to block anaphase A of mitosis. Taxol also causes a number of intriguing secondary effects on interphase cells that are poorly understood. We believed that a bio-active fluorescent taxol derivative could be a useful tool in the study of these cellular mechanisms, especially in interphase cells.

Results: We have synthesized and characterized a series of stable, fluorescently labeled derivatives of taxol that bind to microtubules and have cytotoxicities similar to that of taxol. Fluorescence microscopy experiments in interphase human foreskin fibroblast (HFF) cells indicate that one of these, a sulforhodamine taxoid, is particularly well suited for optical microscopy. The use of this taxoid in HFF cells revealed a previously undetected localization of taxoids to the nucleolus during interphase.

Conclusion: The production of a new fluorescent derivative of taxol provides a useful tool, enabling cellular biologists to study taxol's mechanism of action. It is hoped that this material will prove particularly useful for the study of taxol's effects upon interphase cells.

Addresses: [1]Department of Chemistry and The Skaggs Institute of Chemical Biology, The Scripps Research Institute, 10550 North Torrey Pines Road, La Jolla, California 92037, USA and Department of Chemistry and Biochemistry, University of California at San Diego, 9500 Gilman Drive, La Jolla, California 92093, USA, and [2]Department of Biological Sciences, Dartmouth College, 6044 Gilman, Hanover, New Hampshire 03755, USA.

Correspondence: KC Nicolaou
E-mail: kcn@scripps.edu

Keywords: fluorescence, localization, microscopy, taxol

Received: **5 June 1996**
Revisions requested: **21 June 1996**
Revisions received: **13 November 1996**
Accepted: **22 November 1996**

Chemistry & Biology
December 1996, **3**:1021–1031

Introduction

Taxol [1,2] (compound **1**, Fig. 1) is an anticancer chemotherapeutic agent that was originally isolated in the late 1960's by cytotoxicity-directed fractionation of the methanolic extracts of the bark of the Pacific yew, *Taxus brevifolia* [3]. Although initial studies indicated that the new drug had considerable potential, development was delayed until the 1980's by the scarcity of the natural compound and its apparent lack of advantages over existing treatments [4]. The combination of early preclinical work at the National Cancer Institute (NCI) and the disclosure that taxol had an unusual biochemical mechanism (stabilization of microtubules) by Horwitz and coworkers [5,6], spurred on what became very rapid progression to taxol's current status as a widely used clinical agent. Early on in the clinical trials, researchers observed that the drug had an unusual ability to repress both breast [7] and ovarian [8] cancers. The drug was also shown to have significant effects on several other types of solid tumors including non-small-cell lung and head-and-neck cancers [9].

The study of taxol's mechanism of action has shed light upon the normal process of microtubule dynamics and gives insight into the importance of this process in cellular events [10]. Microtubules are crucial cellular structures. They are composed of heterodimeric tubulin subunits that polymerize to form the multisubunit microtubule, a helical linear polymer 25 nm in diameter with a central 15 nm hole [11,12]. Normally, the microtubules of a cell are in a constant state of flux, growing and shrinking in a manner that has been characterized as 'dynamic instability' [13,14]. The dynamic properties of microtubules are central to many cellular processes, particularly the assembly and function of a mitotic spindle during cell division [15]. Taxol stabilizes the microtubule, preventing 'catastrophe' (the rapid depolymerization of the microtubule to free tubulin subunits) and reducing the amplitude and rate of the changes in microtubule length that are collectively known as 'microtubule dynamics' [16,17].

In cells, the biochemical effects of taxol ultimately lead to a strong inhibition of eukaryotic cell proliferation, usually blocking cell-cycle progression at the G_2/Pro transition into mitosis [18–20]. At this time, the interphase cytoskeleton is disassembled and the microtubules are reorganized into a bipolar array characteristic of the mitotic

*Although in common usage for the last 20 years, Taxol is now a registered trademark of Bristol-Myers Squibb. The copyright of Bristol-Myers Squibb is recognized when Taxol or taxol is used in this article.

Figure 1

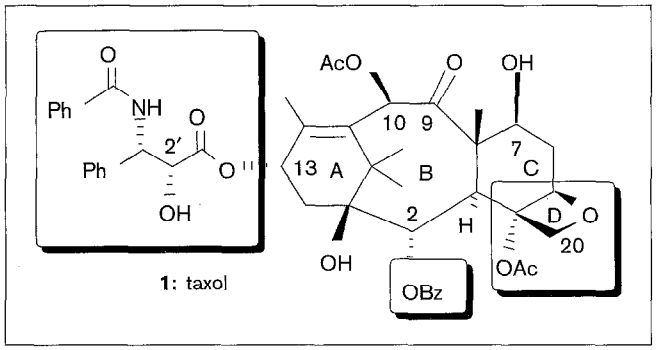

Structure of taxol, compound **1**. The boxed substituents are crucial for biological activity. In reactions with electrophiles, the alcohol at the C2′ position is the most reactive and that at C7 is the second most reactive.

Figure 2

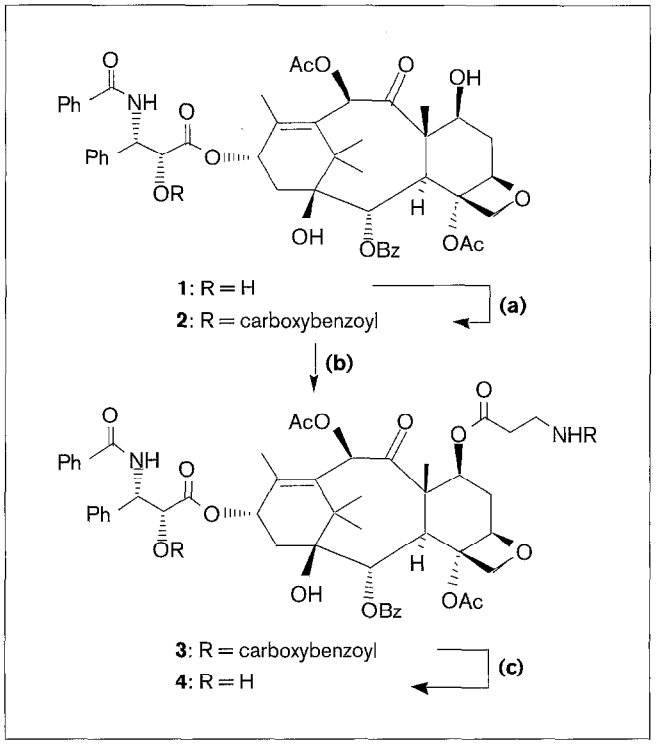

Synthesis of the common reactive intermediate **4**. Reagents and conditions: **(a)** benzyl chloroformate (60 eq. in 10 eq. portions), pyridine (110 eq.), methylene chloride, 25 °C, 70 %; **(b)** N-CBz-β-alanine (4.4 eq.), dicyclohexylcarbodiimide (4.4 eq.), 4-(dimethy-l-amino)pyridine (1 eq.), 25 °C, 18 h, 95 %; **(c)** H_2, 10 % Pd(C) (5 wt. %), MeOH, 25 °C, 2 h, quant.

apparatus. The drug also causes a number of cellular morphological changes in interphase cells [21–25], the most obvious of which is the formation of unusual bundles of microtubules [26–28]. Often, these studies are carried out using optical fluorescence microscopy with either anti-tubulin immunofluorescence or fluorescently labeled tubulin. These techniques require fixation and permeabilization or microinjection, respectively. We envisaged that a bioactive fluorescently labeled derivative of taxol, able to cross the cell membrane, would facilitate the use of fluorescence microscopy techniques. We also expected that such a taxoid would allow the study of previously unprobed areas, such as taxol localization in cells or the presence of a secondary receptor for the drug. In particular, we hoped that such a compound would stimulate work aimed at understanding taxol's effects upon the interphase portion of the cell cycle.

Before this project was begun, no fluorescent derivatives of taxol suitable for fluorescence microscopy had been reported. Kingston [29] had briefly mentioned, with little experimental detail, the production of a C-7 conjugated dansyl derivative of taxol, and Georg and coworkers [30] had reported the production of a sidechain analog of taxol, substituting the weakly fluorescent *m*-dimethylaminobenzoyl group for the normal benzoyl at the C-3′-nitrogen, and its use to study the polarity of the binding site microenvironment. Very recently two groups have reported the preparation of fluorescently labeled taxol [31] and taxotere [32] analogs designed for microscopy.

The design of our targeted derivatives and choice of a synthetic pathway to these compounds followed the outline shown in Figure 2. To allow us to choose the best fluorophore, and to provide a method for linking other spectroscopically active groups (such as those used to enhance magnetic resonance imaging (MRI) and positron emission spectroscopy (PET)), we wished to make all of the desired derivatives using a common reactive intermediate, containing an easily conjugated center. We therefore considered taxol's structure–activity relationship (SAR) [1,2,33] and its known patterns of reactivity. In general, modifications to the sidechain and to the substituents on the 'southern' portion (see boxed regions, Fig. 1) of the molecule are poorly tolerated while changes to the 'northern' portion have little effect upon the drug's activity (see unboxed regions, Fig. 1). Derivatization of the OH group at C-7 of the C-ring of the taxane nucleus to form an ester is usually well tolerated [34–36]. The reactivity of taxol with electrophiles has been well studied [1,2]. The C-2′-hydroxyl of the sidechain is normally the most reactive and can be readily differentiated from the other hydroxyls. When C-2′ is protected, reaction usually proceeds selectively at the C-7 hydroxyl. It was therefore decided to derivatize the C-7 hydroxyl of taxol with an ester that contained a nascent pendant amine. Deutch's group [37] has shown that α-amino esters of this alcohol are fairly unstable. We therefore decided to try to use the β-amino alanine ester as a general linker. To maximize the probability of producing a functional fluorescent taxoid, we explored several different conjugating groups and

Figure 3

Synthesis of fluorescent taxoids **5a-d**. Reagents and conditions: **(a)** dansyl chloride, triethylamine, acetonitrile, 25 °C, 10 min, 69 %; **(b)** fluorescein N-hydroxysuccinate ester, 10 % aqueous sodium bicarbonate, dioxane, 25 °C, 1.2 h, 65 %; **(c)** carboxy-X-rhodamine N-hydroxysuccinate ester, 10 % aqueous sodium bicarbonate, dioxane, 25 °C, 1.5 h, 73 %; **(d)** Lissamine Rhodamine B chloride, 10 % aqueous sodium bicarbonate, dioxane, 25 °C, 2 h.

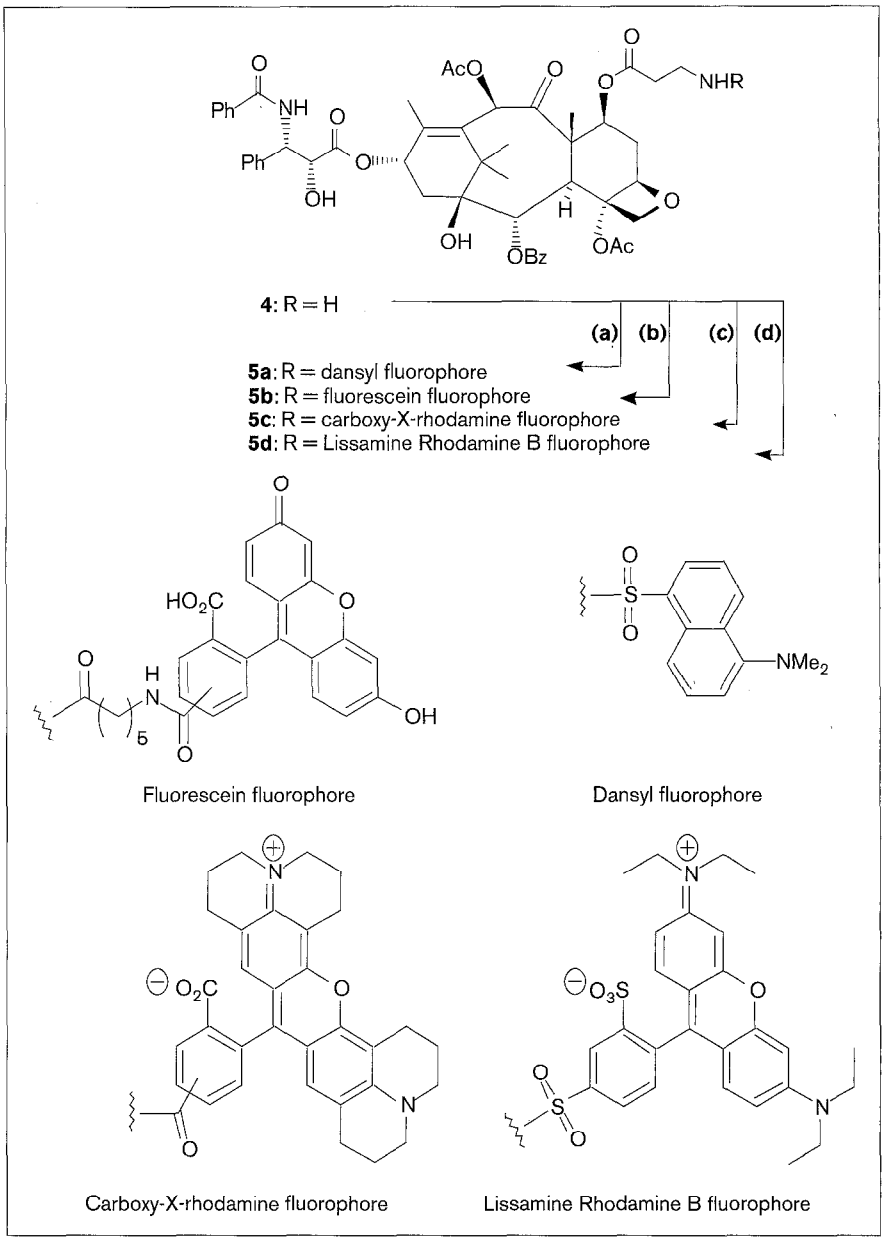

tether lengths for the fluorophores. Because the presence of mixed isomers at the fluorophore's aromatic nucleus does not affect the function of the material in fluorescence microscopy, two of the fluorophores (fluorescein and carboxy-X-rhodamine) were introduced from the commercially available mixture of isomers.

Results and discussion

Synthetic chemistry

With the synthetic goals in mind, taxol (compound **1**, Fig. 1) was reacted with benzyl chloroformate in the presence of pyridine to give the 2′-benzyl carbonate (compound **2**, Fig. 2) of taxol in good (70 %) yield. This was then acylated with N-carboxybenzyl-β-alanine by treating the alcohol with dicyclohexylcarbodiimide and 4-(N,N-dimethylamino)-pyridine to give the ester **3** (Fig. 2) in high (95 %) yield. Concomitant reductive removal of both carboxybenzyl protecting groups gave the desired amine **4** (Fig. 2) in essentially quantitative yield. This amine was then conjugated with several fluorophores in good (65–73 %) yield to give the fluorescently labeled derivatives **5a–d** (Fig. 3).

As mixed isomers pose no problems for fluorescence microscopy, we did not separate the aromatic isomers of the fluorescein and carboxy-X-rhodamine conjugates. The

Table 1

Physical properties of the fluorescent taxoids 5a–d.

	1	5a	5b	5c	5d
Aqueous solubility (M)	$<< 1 \times 10^{-6}$	$<< 1 \times 10^{-6}$	4×10^{-5}	2×10^{-5}	1×10^{-5}
Partition coefficient (n-octanol/water)	> 50	> 50	1	2	2
Fluorescence maxima (nm, excitation/emission)	–	350 / 500	512 / 550	400 / 610 550 / 610	380 / 620 525 / 620

β-alanyl linker proves to be a good 'handle' for conjugation of taxol. The method described above is efficient enough (43–48 % overall yield from taxol) that it is possible to make fluorescent taxoids readily available in any reasonably anticipated quantities for most purposes. The overall method should be easily adaptable to produce other taxol conjugates.

Physical properties

The solubility, stability, and spectroscopic characteristics of the fluorescently labeled taxoids were examined to determine their suitability for further study (Table 1). UV spectroscopic assays show that the three derivatives that contain formal charges, compounds **5b–d**, are significantly more soluble in water than taxol. The dansyl taxoid **5a** retained taxol's highly lipophilic character. The partition coefficients (octanol to water) exhibited a similar shift towards hydrophilic character for the charged derivatives **5b–d**. All the conjugates were reasonably stable in solution (>14 days at room temperature in ethanol (1 mM) with no apparent degradation). Finally, all conjugates retained reasonable excitation/emission spectra (see Table 1) allowing the use of standard filter blocks for fluorescence microscopy. An interesting characteristic of the rhodamine labeled taxoids **5c** and **5d** is that they developed a secondary excitation wavelength after conjugation to the taxoid nucleus. The combination of these characteristics was sufficiently promising to warrant further study.

Tubulin polymerization assays

To test whether the addition of fluorescent groups had impaired the activity of our modified taxoids, we examined their ability to polymerize chick brain tubulin *in vitro* (Fig. 4) [38]. The tubulin used in these assays retained the microtubule-associated proteins (MAPs) [39,40]; this system was viewed as more physiologically relevant. All the taxoids showed enhanced rates of tubulin polymerization and a higher plateau for bulk polymerization levels (as determined when the change of the absorbance reached the level of +0.002/–0.004 A units per min) than the DMSO control. Among the derivatives, the two rhodamine taxoids **5c** and **5d** exhibited the best tubulin polymerization profiles, equaling that of the taxol control within experimental error ±0.002 OD. The fluorescein labeled taxoid **5b** had the next best tubulin-polymerizing ability and the dansyl derivative was least promising.

Figure 4

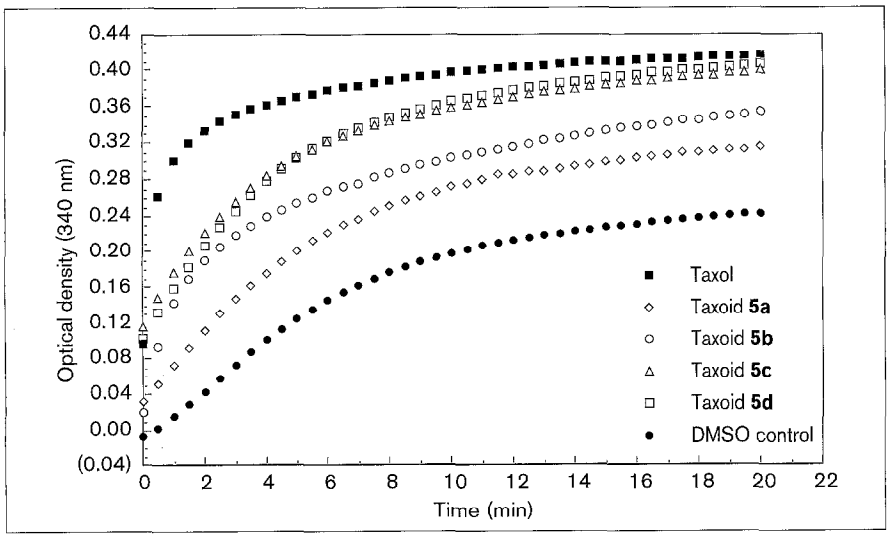

Relative tubulin polymerization abilities of taxol and the fluorescent taxoids **5a–d**. The bulk polymerization was determined by following the change in optical density at 340 nm spectroscopically. For particulars, see Materials and methods.

These results correlate directly with the partition coefficients and aqueous solubility of the respective derivatives, perhaps indicating that profitable interaction with the microtubule requires a group on C-7 that retains the ability to hydrogen bond with bulk water. The observation that these derivatives are slightly less active than taxol is not unexpected, given previous results with other derivatizations at this position [32]. All of the fluorescent taxoids retain enough binding to microtubules that it is reasonable to expect them to be active *in vivo*.

Cytotoxicity assays

To evaluate how well the fluorescently labeled taxoids retained their cytotoxicity, the derivatives were tested for their ability to inhibit the growth [41] of two cell lines: Chinese hamster ovary (CHO) and HeLa cervical carcinoma (HeLa) (Fig. 5). All the derivatives had significant entotoxic effects, though attenuated relative to taxol. This trend held for both cell lines, although the magnitude of growth inhibition was much lower in the CHO line (as expected since this cell line is normally less sensitive to taxoids than HeLa). The dansyl taxoid, **5a,** showed the highest cytotoxicity. The two rhodamine derivatives (**5c** and **d)** had approximately equal cytotoxicities that were less than that of the dansyl taxoid, and the fluorescein derivative had the lowest cytotoxicity of the four. These results can not be directly related to either partition coefficient or aqueous solubility. All the charged derivatives have lower cytotoxicities than the uncharged derivative or the taxol control, however. This may be because the

Figure 5

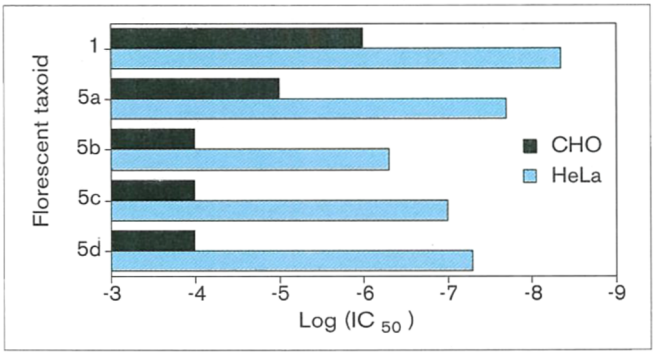

Relative cytotoxicities of taxol (**1**) and the fluorescent taxoids **5a–d**. The cytotoxicities were determined using the standard XTT assay. For particulars, see Materials and methods.

Figure 6

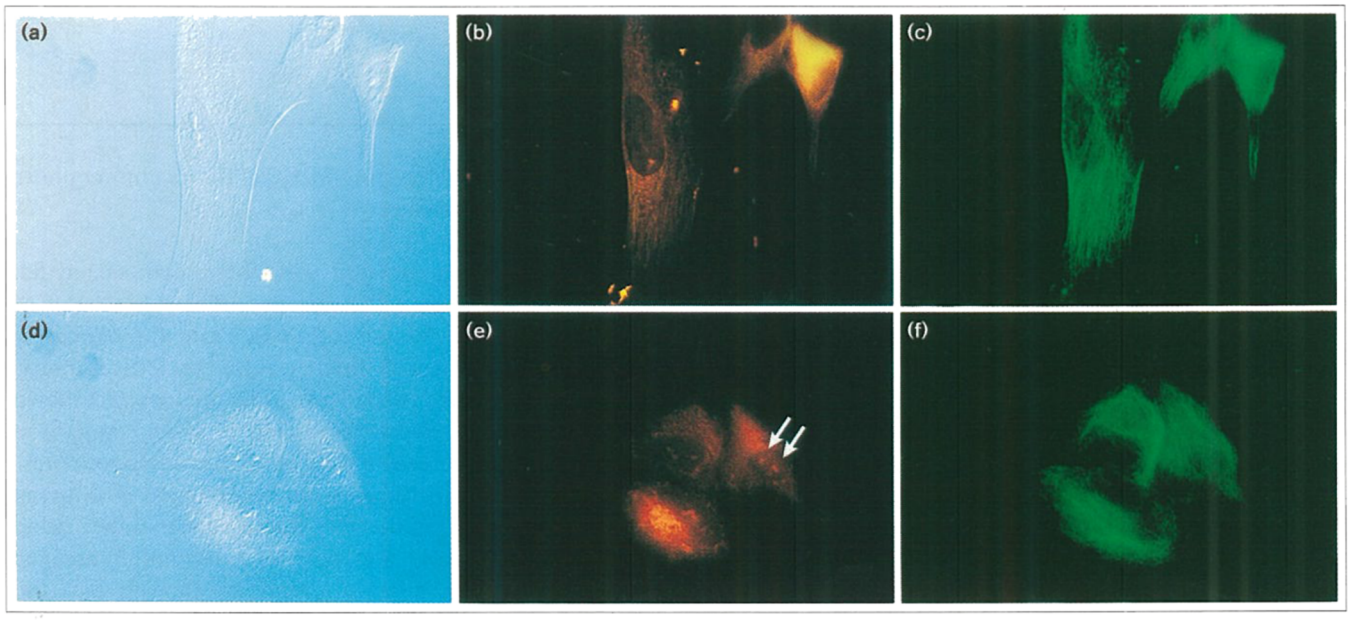

Microscopy images of human foreskin fibroblasts after exposure to Lissamine Red taxoid **5d** (all cells have been fixed to allow comparison with the controls). **(a)** DIC photomicrograph showing normal cellular morphology after 1 h exposure to the drug (20 μM, 37 °C). **(b)** Fluorescence photomicrograph of the same field shown in (a), using the rhodamine filter set, showing the fluorescence signal of the taxoid **5d**. **(c)** Fluorescence photomicrograph of the same field shown in (a), using the fluorescein filter set, showing the microtubule cytoskeleton, as illuminated by traditional immunofluorescence using an α-tubulin monoclonal. **(d)** DIC photomicrograph showing the abnormal cellular morphology that develops after 24 h exposure to taxoid **5d** (20 μM, 37 °C). **(e)** Fluorescence photomicrograph of the same field shown in (d) showing the fluorescence signal of the taxoid. Note the small structures of localized fluorescence (nucleoli marked by arrows) that do not appear in the immunofluorescence control. **(f)** Fluorescence photomicrograph of the same field shown in (d) showing the microtubule cytoskeleton by traditional immunofluorescence after 24 h exposure (note the absence of nucleoli). Clearly, in general the fluorescent taxoid reveals the same cytoskeletal structures as does traditional immunofluorescence. For experimental details, see Materials and methods.

Figure 7

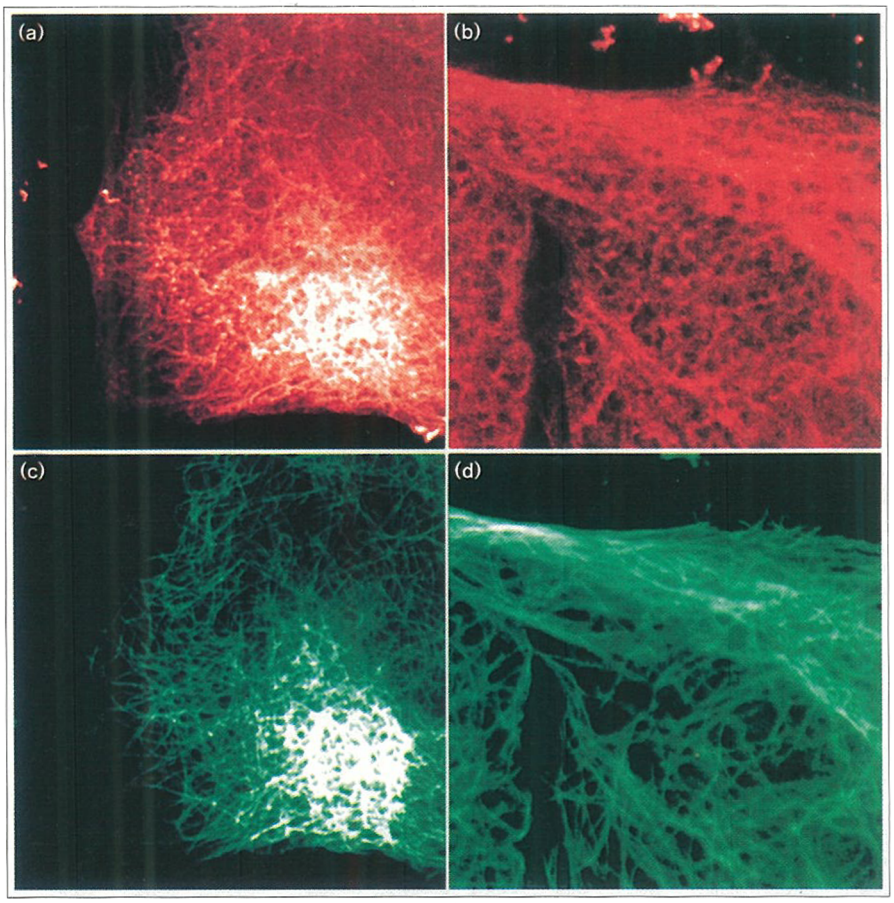

Confocal microscopy images of human foreskin fibroblasts after 1 h exposure to Lissamine Red taxoid **5d** (20 μM, 37 °C, cells were fixed to allow comparison to the controls). The instrument was configured for blue to far red fluorescence excitation (458, 568 and 647 nm) enabling three-color confocal imaging of cells directly. **(a)** The rhodamine signal. Note the high degree of detail revealed by the Lissamine taxoid **5d** relative to the controls. **(b)** Electronic magnification (2×) of a portion of (a) showing the fine details that are visualized by taxoid **5d**. **(c)** Fluorescence photomicrographs of the same field shown in (a), using the fluorescein filter set, showing the fluorescence signal from a traditional immunofluorescence α-tubulin monoclonal). **(d)** Electronic magnification (2×) of a portion of (c). For experimental details, see Materials and methods

charged derivatives diffuse less well across the hydrophobic cell membrane, as observed previously with other charged derivatives at this position [42]. These results, combined with those from the experiments described above, clearly indicated that the rhodamine derivatives are the most promising for microscopy.

Fluorescence microscopy

We performed fluorescence microscopy experiments with three taxoids, the two rhodamine-labeled taxoids and the fluorescein-labeled one. These studies used cultured human foreskin fibroblasts, chosen because they become quiescent due to contact inhibition when well spread on the cover slips. In this state they have a clearly visible interphase array of microtubules. They therefore provide a good model for interphase cells, which these taxoids were designed to study. The fluorescein taxoid **5b** exhibited rapid photobleaching and was not pursued further. Both the carboxy-X-rhodamine **5c** and Lissamine **5d** taxoids had reasonable amplitudes of fluorescence and fluorescence lifetimes. Most of the microscopy studies were carried out using the Lissamine-labeled taxoid, because it has a slightly higher tubulin polymerization ability and cytotoxicity, a slightly cleaner fluorescence appearance, and the starting material for its chromophore is relatively inexpensive.

When the cells were treated with fluorescent taxoid **5d**, they began to display fluorescent cellular networks of microtubules after ~10 min (Fig. 6b), a rate approximately equal to that with which fluorescently labeled tubulin is incoporated into the cytoskeleton. The micrographs shown in Figures 6 and 7 depict fixed cells to allow comparison between the fluorescent taxoid and the immunofluorescence control. Similar images can be obtained with living cells (see Fig. 8). Double label fluorescence studies using the fluorescent taxoid and indirect immunofluorescence with anti-α-tubulin primary antibodies showed that the derivatives illuminate the same microtubule skeleton as does traditional immunofluorescence (Fig. 6c), and that the derivative does not block the binding of these antibodies to microtubules. The level of signal from the fluorescent taxoid **5d** is higher than that from the antibody controls (see Fig. 7). The most likely explanation for this is that, under the experimental conditions employed, the taxoid (at 20 μM) has saturated the binding sites of the microtubules (previously estimated at 10–20 μM, E.D. Salmon, personal communication) while the anti-α-tubulin

antibody has not and therefore gives a weaker signal. There is also some evidence of a diffuse background signal that may represent unbound taxoid or agent bound to small tubulin oligomers. Given the degree of overall tubulin polymerization demonstrated by the Lissamine taxoid **5d** *in vitro*, it is more likely that the background signal is due to small oligomers. Thus, the net result of visualization with Lissamine taxoid **5d** is a more richly detailed image than that provided by immunofluorescence. It is important to note that, unlike immunofluorescence images, these images can be obtained from living cells.

Cells treated with fluorescent taxoids retained normal morphology (Fig. 6a) and microtubule networks (Fig. 6b) for ~90–120 min, after which the cells appeared progressively abnormal by differential interference contrast (DIC) microscopy. After 20 h of treatment with the fluorescent derivative, the long extensions of the cells had retracted somewhat (Fig. 6d) and their microtubule networks appeared more bundled than filamentous (Fig. 6e). These results are as expected for a human cancer cell line treated with a taxoid. They demonstrate that the fluorescent conjugation of taxol does not significantly perturb the behavior of these derivatives in living cells. It is therefore reasonable to assume that such compounds could be used to study taxol's cellular mechanism of action. The synthetic chemistry described here is generally applicable to all taxoids containing a C-7 hydroxyl group, allowing this method of conjugation to be adapted to specific taxoids of interest. This class of derivatives should therefore enable workers to examine differences in the cellular behavior of specific taxoids with different physiological effects, especially in interphase cells.

In the cells that had been treated with taxoids **5c** and **5d** for an extended period of time, some of the taxoid appears to have partitioned into structures that do not include tubulin. These structures include nucleoli (see those marked by arrows in Fig. 6e and 8) and, occasionally, small punctate objects. Immunofluorescence controls revealed no co-localization of α-tubulin antibodies for either type of partitioning and therefore, if these structures contain microtubules the tubulin epitope must no longer be accessible to the α-tubulin antibody.

The punctate structures that occasionally form in the cytoplasm may be small asters of microtubules; these are microtubule structures that have been observed by DIC microscopy in taxol-treated sea urchin eggs [43]. A more likely explanation for this phenomenon, however, is that the punctate structures are inclusion bodies into which the taxoids have been segregated in an effort to reduce their toxic effects. Taxol is more effective at killing cancer cells *in vitro* when administered as a slow infusion over 6–24 h [44]. It may be that inclusion body formation explains this empirical observation; perhaps inclusion bodies form only when too much drug is delivered in a given period. Alternatively, the fluorophore itself could be causing the segregation. A final possibility could be that the punctate structures are not securely fixed and are washed away during the immunofluorescence staining.

Figure 8

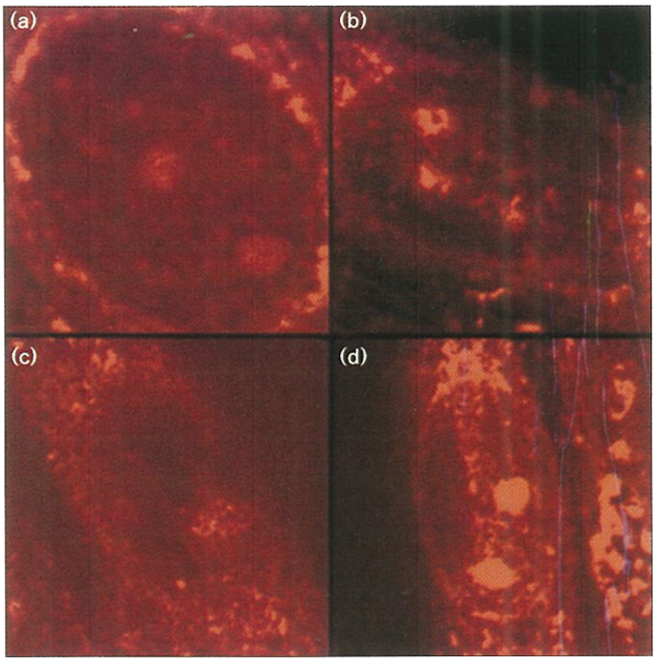

Competition between unlabeled taxol **1** and Lissamine-labeled taxoid **5d** for intracellular binding sites. The series of experiments shows that staining of the nucleoli is retained despite competition by unlabeled taxol. The figure depicts confocal microscopy images of human foreskin fibroblasts after 24 h exposure to a mixture of taxol **1** and Lissamine taxoid **5d** (20 μM overall taxoid concentration, held constant in all experiments, 37 °C, cells are living and unfixed). The instrument was configured for far red fluorescence excitation. **(a)** The rhodamine signal generated by 100 % Lissamine taxoid **5d**. Note the staining of nucleoli (globular structures in the nucleus). **(b)** A 3:1 mixture of taxol **1** and Lissamine taxoid **5d**. The relative level of signal between the microtubule based cytoskeleton and the nucleoli remains the same as in (a). **(c)** A 1:1 mixture of **1** and **5d**. **(d)** A 1:3 mixture of **1** and **5d**. The images in (c) and (d) were produced by photon accumulation and software control on the confocal microscope. This technique allowed the observation of the otherwise extremely weak overall fluorescence signal from the dilute Lissamine taxoid **5d**. For experimental detail, see Materials and methods.

The main fluorescence signal other than that due to tubulin distribution is the nucleolus which regularly exhibits fluorescence after exposure to **5d**. There is no evidence for the presence of microtubules or tubulin in the nucleolus, but there is good evidence that one class of MAPs (the tau proteins) is present in the nucleolus of certain vertebrate tissue culture cells [45,46]. As the nucleolus is not a membrane-bound organelle, the fact that the relatively hydrophobic taxoid **5d** accumulates within it cannot be explained by partitioning of the hydrophobic

taxane into a membrane. In competition experiments with constant (20 μM) levels of total taxol and decreasing proportions of labeled taxol **5d** the relative levels of signal from the nucleolus and cytoskeleton remained constant (see Fig. 6). This result indicates that the binding of taxoid **5d** to the nucleolus is as least as specific as its binding to the microtubule cytoskeleton. There are two reasonable explanations for this observation: there may be previously undetected tubulin subunits in the nucleolus itself during interphase, or the nucleolus may contain a previously undetected receptor for taxol other than microtubules. As the evidence against the presence of microtubules in the nucleus is strong, the second explaination seems most plausible. The potential of a new receptor for taxol raises interesting possibilities for further study.

Significance

The work presented above shows that the C-7 position of taxol can be substituted with a variety of groups attached via a β-alanyl ester linker. These studies have defined a general synthetic route to taxoids of this type that proceeds with good overall yield. The method should easily adapt to the production of any labeled taxoid of interest. According to these studies, substitutions at the C-7 position of the taxane nucleus retain reasonable biological activity. In this study, we made a bioactive fluorescent derivative of taxol, **5d**, that is useful for fluorescence microscopy. This derivative allows study of the microtubule-based cytoskeleton of living cells without using invasive techniques such as the microinjection of fluorescently labeled proteins or the more severe fixation procedures required for immunofluorescence. The inherently high level of signal provided by using a large excess of a freely-diffusible specific fluorophore, such as **5d**, provides a more detailed image than traditional immunofluorescence. It is hoped that these derivatives will prove useful for researchers who are examining the dynamic properties of microtubules in cells. In particular, we hope that these derivatives will enable studies of the effects of taxol in the relatively untouched area of interphase cells. These derivatives have already revealed the subcellular localization of taxoids to the nucleolus — an unanticipated and intriguing result.

Materials and methods

Chemistry

General techniques

All reactions were carried out in an argon atmosphere with freshly dried solvents under anhydrous conditions, unless otherwise noted. All reagents were purchased at highest commercial quality and used without further purification, unless otherwise stated. Preparative scale high performance liquid chromatography (HPLC) was carried out using a Vydak RP-18 (22.5 mm by 250 mm) column with a flow rate of 9 ml min^{-1} and UV detection at 254 nm. NMR spectra were recorded on a Bruker AMX-500 instrument and calibrated using residual undeuterated solvent as an internal reference. The following abbreviations were used: s, singlet; d, doublet; t, triplet; m, multiplet; band, several overlapping signals; br, broad. The carbon numbering of taxol was used to assign protons. Overlapping carbon signals were reported only once. Infrared (IR) spectra were recorded on a Perkin-Elmer 1600 series FT-IR spectrometer. High resolution mass spectra (HRMS) were recorded on a VG ZAB-ZSE mass spectrometer under fast atom bombardment (FAB) conditions.

2′-Carboxybenzoyltaxol ***2***

A solution of taxol **(1)** (100 mg, 0.117 mmol) and pyridine (950 μl, 11.7 mmol, 100 equivalent (eq.)) in methylene chloride (5 ml) at room temperature under argon was treated, at 10 min intervals, with benzyl chloroformate (170 μl aliquots, 1.17 mmol, 10 eq. to total of 60 eq.). When thin layer chromatography (TLC) (silica, 50 % EtOAc in hexanes, UV/PMA) showed no remaining starting material, the reaction was quenched with aqueous NH_4Cl (1 ml). After dilution with ethyl acetate (10 ml), the reaction mixture was washed with ammonium chloride (2 × 5 ml), copper sulfate (4 × 10 ml), and sodium chloride (5 ml). The combined organic layer was dried (Na_2SO_4), concentrated, and purified by flash chromatography (silica, 50 % EtOAc in hexanes) to give 2′-carboxybenzoyltaxol as a white powder (80 mg, 70 %): $R_f = 0.50$ (silica, 50 % EtOAc in hexanes); Tg (glass transition) = 152–154 °C; melting point (mp) = 206–210 °C; $[\alpha]^{24}D$ −53.8 (c 0.01 g ml^{-1}, $CHCl_3$); IR (thin film) ν_{max} 1240, 1371, 1724, 2962, 3511 cm^{-1}; ^1H NMR (500 MHz, $CDCl_3$) δ, 1.14 (s, 3 H, 16-H), 1.25 (s, 3 H, 17-H), 1.69 (s, 3 H, 19-H), 1.76 (s, 1 H, 1-OH), 1.93 (s, 3 H, 18-H), 1.9–1.94 (m, 1 H, 6β-H), 2.2–2.3, 2.4–2.5 (m, 2 H, 14-H), 2.24 (s, 3 H, 10-OAc-H), 2.46 (s, 3 H, 4-OAc-H), 2.51 (s, 1 H, 7-OH), 2.60 (m, 1 H, 6α-H), 3.82 (d, $J = 7$, 1 H, 3-H) 4.20 (d, $J = 8.5$, 1 H, 20-H, A of AB), 4.32 (d, $J = 8.5$, 1 H, 20-H, B of AB), 4.41 (m, 1 H, 7-H), 4.98 (d, $J = 8$, 1 H, 5-H), 5.18 (dd, $J = 9,10$, 2 H, Bn, AB), 5.45 (d, $J = 2.5$, 1 H, 2′-H), 5.69 (d, J = 7, 1 H, 2-H), 5.98 (dd, $J = 2.5, 9.5$, 1 H, 3′-H), 6.30 (band, 2 H, 10-H, 13-H), 6.92 (d, $J = 9.5$, 1 H, NH), 7.30–7.42 (band, 12 H, Ar-H), 7.44–7.54 (band, 3 H, Ar-H), 7.61 (t, $J = 7$, 1 H, Ar-H), 7.73 (d, $J = 8.5$, 2 H, Bz-H), 8.14 (d, $J = 8.5$, 2 H, Bz-H); ^{13}C NMR (125 MHz, $CDCl_3$) δ 9.5, 14.7, 20.7, 22.0, 22.6, 26.7, 35.4, 35.5, 40.5, 44.4, 45.4, 52.6, 58.2, 70.7, 71.9, 72.0, 74.9, 75.5, 76.3, 76.7, 78.1, 81.2, 84.3, 126.5, 127.0, 128.3, 128.4, 130.1, 131.9, 132.1, 133.0, 134.0, 137.2, 142.5, 154.1, 166.9, 167.2, 168.8, 171.1, 204.1; FAB HRMS (NBA/CsI) *m/e* found: 1121.2852 ($M + Cs^+$); calc'd for $C_{55}H_{57}NO_{16}Cs$: 1121.2810.

2′-Carboxybenzoyl-7-(N-carboxybenzoyl-β-alanyl)-taxol ***3***

A solution of 2′-carboxybenzoyltaxol **2** (25 mg, 0.025 mmol) and 4-(N,N-dimethylamino)-pyridine (3 mg, 0.025 mmol, 1 eq.) in methylene chloride (2 ml) at room temperature under argon was treated with N-carboxybenzoyl-β-alanine (24 mg, 0.11 mmol, 4.4 eq.) and dicyclohexycarbodiimide (22 mg, 0.11 mmol, 4.4 eq.). After 18 h, the mixture was diluted with methylene chloride (5 ml) and filtered to remove the urea. The crude product was evaporated to dryness *in vacuo* and purified by flash chromatography (silica, 40–45 % EtOAc in hexanes) to give 2′-carboxybenzoyl-7-(N-carboxybenzoyl-β-alanyl)-taxol as a white powder (28 mg, 95 %): $R_f = 0.55$ (silica, 50 % EtOAc in hexanes); mp = 114–116 °C; $[\alpha]^{24}_D$ −45.7 (c 0.01 g ml^{-1}, $CHCl_3$); IR (thin film) ν_{max} 1176, 1240, 1372, 1651, 1728, 1747, 2936, 3401 cm^{-1}; ^1H NMR (500 MHz, $CDCl_3$) δ, 1.15 (s, 3 H, 16-H), 1.21 (s, 3 H, 17-H), 1.81 (s, 3 H, 19-H), 1.99 (s, 3 H, 18-H), 2.06 (s, 3 H, 10-OAc-H), 2.21 (m, 1 H, 6β-H), 2.4–2.6 (band, 5 H, 14-H, 6α-H, alanyl CH_2), 2.46 (s, 3 H, 4-OAc-H), 3.4–3.5 (m, 2 H, alanyl CH_2), 3.96 (d, $J = 7$, 1 H, 3-H), 4.20 (d, $J = 8.5$, 1 H, 20-H, A of AB), 4.33 (d, $J = 8.5$, 1 H, 20-H, B of AB), 4.95 (d, $J = 8.5$, 1 H, 5-H), 5.18 (dd, $J = 9,10$, 2 H, Bn, AB), 5.45 (d, $J = 2.5$, 1 H, 2′-H), 5.63 (dd, $J = 5.7$, 1 H, 7-H), 5.70 (d, $J = 7$, 1 H, 2-H), 5.98 (dd, $J = 2.5, 9$, 1 H, 3′-H), 6.22–6.30 (band, 2 H, 10-H, 13-H), 6.98 (d, $J = 9$, 1 H, NH), 7.30–7.42 (band, 17 H, Ar-H), 7.43–7.52 (band, 3 H, Ar-H), 7.61 (t, $J = 7$, 1 H, Ar-H), 7.73 (d, $J = 8.5$, 2 H, Bz-H), 8.14 (d, $J = 8.5$, 2 H, Bz-H); ^{13}C NMR (125 MHz, $CDCl_3$) δ 10.8, 14.4, 20.4, 21.3, 22.5, 24.8, 25.5, 26.3, 33.3, 33.8, 34.2, 35.3, 43.1, 46.5, 48.2, 52.7, 55.9, 66.3, 70.7, 71.4, 71.9, 74.4, 75.2, 76.6, 77.2, 78.5, 80.7, 83.7, 126.5, 127.0, 127.8, 128.0, 128.4, 128.6, 128.8, 128.9, 130.1, 131.9, 132.4, 133.4, 133.6, 136.6, 141.2, 153.9, 156.2, 166.8, 167.1, 167.8, 169.4, 169.6, 171.0, 202.1; FAB HRMS (NBA/CsI) *m/e* found: 1326.3553 ($M + Cs^+$); calc'd for $C_{66}H_{68}N_2O_{19}Cs$: 1326.3549.

7-β-alanyltaxol ***4***

A solution of compound **3** (25 mg, 0.021 mmol) in methanol (1 ml) at room temperature under argon was treated with 10 % palladium on carbon (1 mg, 4 wt %) and placed under hydrogen. After 2 h, the mixture was filtered to remove the catalyst and evaporated to dryness *in vacuo* to give 7-β-alanyltaxol **4** as a white powder (19 mg, quant.): mp = 215–218 °C; R_f = 0.55 (silica, 10 % MeOH in methylene chloride); $[\alpha]^{24}D$ −42.1 (*c* 0.01 g ml^{-1}, $CHCl_3$); IR (thin film) ν_{max} 1176, 1240, 1412, 1662, 1716, 1765, 2990, 3301, 3482 cm^{-1}; ^{1}H NMR (500 MHz, CD_3OD) δ, 1.09 (s, 3 H, 16-H), 1.16 (s, 3 H, 17-H), 1.78 (s, 3 H, 19-H), 1.78–1.89 (m, 1 H, 6β-H), 1.87 (s, 3 H, 18-H), 1.91–2.00 (m, 1 H, 14-H), 2.18 (s, 3 H, 10-OAc-H), 2.19–2.24 (m, 1 H, 14-H), 2.38 (s, 3 H, 4-OAc-H), 2.50–2.59 (m, 1 H, 6α-H), 2.65–2.67 (m, 2 H, alanyl CH_2), 3.12–3.22 (m, 2 H, alanyl CH_2), 3.90 (d, *J* = 7, 1 H, 3-H) 4.19 (dd, *J* = 7, 14, 2 H, 20-H), 4.73 (d, *J* = 6, 1 H, 2′-H), 5.00 (d, *J* = 8.5, 1 H, 5-H), 5.63–5.65 (band, 3 H, 2-H, 3′-H, 7-H), 6.14 (br t, *J* = 6, 1 H, 13-H), 6.19 (s, 1 H, 10-H), 7.28–7.67 (band, 11 H, Ar-H, NH), 7.85 (dd, *J* = 1.5, 7.5, 2 H, Bz-H), 8.14 (dd, *J* = 1.5,7.5, 2 H, Bz-H); ^{13}C NMR (125 MHz, CD_3OD) δ 11.4, 14.7, 20.8, 22.1, 23.2, 25.4, 26.7, 32.4, 36.3, 36.5, 44.6, 47.9, 49.2, 57.2, 57.7, 72.1, 73.6, 74.9, 75.8, 76.9, 77.3, 78.8, 80.0, 81.8, 85.0, 128.5, 129.0, 129.6, 129.7, 131.2, 132.9, 134.1, 134.7, 135.6, 139.9, 142.4, 167.6, 170.3, 171.3, 171.8, 172.2, 174.5, 203.7; FAB HRMS (NBA/CsI) *m/e* found: 1057.2765 (M + Cs^+); calc'd for $C_{50}H_{56}N_2O_{15}Cs$: 1057.2735.

Dansyl taxoid ***5a***

A solution of compound **4** (4.6 mg, 0.005 mmol) and triethylamine (1 μl, 0.0075 mmol, 1.5 eq.) in acetonitrile (1 ml) at room temperature under argon was treated with dansyl chloride (2 mg, 0.007 mmol, 1.4 eq). After 10 min, the solvent was removed *in vacuo* and the residue was purified by flash chromatography (silica, 50 % EtOAc in hexanes) to give **5a** as a white powder (4 mg, 69 %): mp = 208–210 °C; R_f = 0.29 (silica, 50 % EtOAc in hexanes); IR (thin film) ν_{max} 1096, 1382, 1474, 1522, 1744, 1748, 1793, 2958, 3109 cm^{-1}; ^{1}H NMR (500 MHz, $CDCl_3$) δ, 1.12 (s, 3 H, 16-H), 1.19 (s, 3 H, 17-H), 1.73 (s, 3 H, 19-H), 1.78 (s, 3 H, 18-H),1.91–2.00, (m, 1 H, 6β-H), 2.15 (s, 3 H, 10-OAc-H), 2.22–2.30 (m, 2 H, 14-H), 2.37 (s, 3 H, 4-OAc-H), 2.50–2.59, (m, 1 H, 6α-H), 2.86 (s, 6 H, NMe-H), 3.20 (m, 2 H, alanyl CH_2), 3.41–3.49 (m, 2 H, alanyl CH_2), 3.86 (d, *J* = 7, 1 H, 3-H), 4.14 (d, *J* = 8, 1 H, 20-H, A of AB), 4.29 (d, *J* = 8, 1 H, 20-H, B of AB), 4.79 (b m, 1 H, 2′-H), 4.87 (d, *J* = 9, 1 H, 5-H), 5.50 (dd, *J* = 7, 10, 1 H, 7-H), 5.64 (d, *J* = 7, 1 H, 2-H), 5.77 (dd, *J* = 2.5, 8, 1 H, 3′-H), 5.87 (br t, *J* = 6, 1 H, 13-H), 6.17 (s, 1 H, 10-H), 6.18 (br m, 1 H, NH), 7.02 (d, *J* = 9, 1 H, NH), 7.16 (d, 1 H, *J* = 7.5, Ar-H), 7.29–7.60 (m, 13 H, Ar-H), 7.74 (d, *J* = 7.5, 2 H, Bz-H), 8.09 (d, *J* = 7.5, 2 H, Bz-H), 8.22 (d, *J* = 7.5, 1 H, Ar-H), 8.31 (d, *J* = 8.5, 1 H, Ar-H), 8.50 (d, *J* = 8.5, 1 H, Ar-H); ^{13}C NMR (125 MHz, $CDCl_3$) δ 9.4, 10.7, 14.5, 20.7, 20.8, 20.8, 22.4, 24.8, 25.5, 26.4, 29.6, 33.2, 33.8, 33.9, 35.4, 38.1, 43.0, 45.3, 46.6, 49.0, 54.8, 55.9, 66.4, 71.6, 72.1, 73.0, 74.1, 75.2, 78.4, 80.6, 83.6, 115.0, 119.0, 123.1, 126.9, 128.0, 128.3, 128.6, 128.9, 128.9, 129.0, 129.6, 129.8, 130.0, 131.9, 132.7, 133.5, 133.7, 135.2, 137.8, 140.5, 151.7, 166.8, 169.8, 170.3, 170.8, 172.4, 201.8; FAB HRMS (NBA/CsI) *m/e* found: 1290.3288 (M + Cs^+); calc'd for $C_{62}H_{67}N_3SO_{17}Cs$: 1290.3246.

Fluorescein taxoid ***5b***

A solution of compound **4** (7.4 mg, 0.008 mmol) in 1:1 dioxane:saturated aqueous sodium bicarbonate (1 ml) at room temperature under argon was treated with 6-(fluorescein-5-(and 6)-carboxamidehexanoic acid succinimidyl ester (5 mg, 0.009 mmol, 1.1 eq). After 1.2 h, the solvent was removed *in vacuo* and the residue was purified by flash chromatography (silica, 1 % AcOH and 10 % MeOH in methylene chloride) to give **5b** as a yellow film (7 mg, 65 %): mp = 300 °C (dec.); R_f = 0.41 (silica, 1 % AcOH and 10 % MeOH in methylene chloride); IR (thin film) ν_{max} 1112, 1451, 1620, 1728, 1734, 2980, 3000, 3401 cm^{-1}; ^{1}H NMR (500 MHz, 1:1 $CDCl_3$:CD_3OD) δ, 0.93 (s, 3 H, 16-H), 0.97 (s, 3 H, 17-H), 1.15–1.22 (m, 2 H, CH_2), 1.40–1.50 (m, 4 H, CH_2), 1.59 (s, 3 H, 19-H), 1.60–1.63 (m, 1 H, 6β-H), 1.79 (s, 3 H, 18-H), 1.97 (s, 3 H, 10-OAc-H), 1.98–2.03 (m, 4 H, CH_2), 2.08–2.16 (m, 2 H, 14-H), 2.17 (s, 3 H, 4-OAc-H), 2.26–2.40 (band, 3 H, 6α-H, CH_2), 3.16–3.30 (m, 2 H, alanyl CH_2), 3.69 (d, *J* = 7, 1 H, 3-H), 4.01 (d, *J* = 8.5, 1 H, 20-H, A of AB), 4.09 (d, *J* = 8.5, 1 H, 20-H, B of AB), 4.55 (brm, 1 H, 2′-H), 4.74 (d, *J* = 9, 1 H, 5-H), 5.38 (dd, *J* = 7, 10, 1 H, 7-H), 5.48 (d, *J* = 7, 1 H, 2-H), 5.50 (m, 1 H, 3′-H), 5.96 (br t, *J* = 9, 1 H, 13-H), 6.03 (s, 1 H, 10-H), 6.28–6.39 (band, 4 H, ArH), 6.98 (br t, *J* = 7, 1 H, NH), 7.02 (d, *J* = 8, 1 H, Ar-H), 7.10 (m, 1 H, N-H), 7.15–7.32 (band, 10 H, Ar-H, NH), 7.57 (d, *J* = 7.5, 2 H, Ar-H), 7.89 (d, *J* = 7.5, 2 H, Bz-H), 7.97 (dd, *J* = 1.5, 7, 2 H, Ar-H), 8.15 (bt, *J* = 6, 1 H, Ar-H), 8.21 (s, 1 H, Ar-H); ^{13}C NMR (125 MHz, 1:1 $CDCl_3$:CD_3OD) δ 11.0, 14.0, 20.8, 21.0, 22.5, 24.6, 25.9, 26.0, 28.2, 33.1, 33.2, 33.9, 34.0, 35.1, 35.7, 35.8, 39.1, 39.3, 39.5, 39.9, 43.3, 47.2, 50.8, 51.0, 55.1, 56.0, 72.2, 72.3, 72.8, 74.0, 75.3, 76.1, 79.8, 80.7, 83.2, 102.5, 126.4, 127.2, 128.0, 128.1, 128.2, 128.3,128.3, 128.4, 129.4, 131.8, 132.4, 133.0, 140.7, 141.2, 166.4, 166.6, 170.0, 171.0, 178.8, 199.1, 202.4; FAB HRMS (NBA/CsI) *m/e* found: 1528.4010 (M + Cs^+); calc'd for $C_{77}H_{77}N_3O_{22}Cs$: 1528.4053.

Carboxyrhodamine taxoid ***5c***

A solution of compund **4** (7.4 mg, 0.008 mmol) in 1:1 dioxane:saturated aqueous sodium bicarbonate (1 ml) at room temperature under argon was treated with (5-(and 6-)carboxysuccinimidyl ester)-2-carboxyrhodamine (6 mg, 0.009 mmol, 1.1 eq). After 1.5 h, the solvent was removed *in vacuo* and the residue was purified by HPLC (a gradient of 80 % 20 mM ammonium acetate in methanol to 100 % methanol over 30 min) to give **5b** as a red film (8 mg, 73 %): mp = 252–256 °C (dec.); R_f = 0.58 (silica, 1 % AcOH and 10 % MeOH in methylene chloride); IR (thin film) ν_{max} 1064, 1156, 1550, 1601, 1720, 1756, 2986, 3690 cm^{-1}; ^{1}H NMR (500 MHz, CD_3OD) δ, 0.85–0.95 (m, 4 H, CH_2), 1.06 (s, 3 H, 16-H), 1.14 (s, 3 H, 17-H), 1.20–1.41 (m, 4 H, CH_2), 1.76 (s, 3 H, 19-H), 1.89 (s, 3 H, 18-H), 2.05 (m, 1 H, 6β-H), 2.06 (m, 2 H, CH_2), 2.09 (s, 3 H, 10-OAc-H), 2.35 (s, 3 H, 4-OAc-H), 2.51–2.70 (band, 3 H, CH_2, 6α-H), 3.01–3.04 (m, 2 H, CH_2), 3.41–3.71 (m, 6 H, CH_2), 3.91 (d, *J* = 7, 1 H, 3-H), 4.16 (d, *J* = 8.5, 1 H, 20-H, A of AB), 4.28 (d, *J* = 8.5, 1 H, 20-H, B of AB), 4.48 (brm, 1 H, 2′-H), 4.74 (d, *J* = 9, 1 H, 5-H), 5.60 (band, 3 H, 2-H, 3′-H, 7-H), 6.12 (br t, *J* = 9, 1 H, 13-H), 6.22 (s, 1 H, 10-H), 6.73 (d, *J* = 7.5, 1 H, Ar-H), 7.25 (br t, *J* = 9, 1 H, NH), 7.40–7.72 (band, 13 H, ArH), 7.81 (d, *J* = 8, 1 H, Ar-H), 8.00 (d, *J* = 9, 1 H, Ar-H), 8.12 (d, *J* = 7.5, 2 H, Ar-H), 8.44 (s, 1 H, Ar-H); ^{13}C NMR (125 MHz, CD_3OD) δ 11.0, 13.1, 14.7, 20–21 (m), 22.0, 25.1, 25.3, 28–29 (m), 30.2, 31.3, 43.0, 50.1, 51.5, 55.1, 56.0, 65.1, 100.2, 104.7, 110.6, 111.3, 114.0, 119.3, 122.4, 124.0, 125.7, 126.0, 126.4, 127.0, 127.1, 127.3, 128.2, 129.0, 130.3, 131.4, 133.2, 133.4, 134.7, 151.2, 152.0, 158.0, 166.3, 168.0, 169.2, 171.1, 173.4, 206.2; positive electrospray *m/e* found: 1442.6, (M + H^+); calc'd for $C_{83}H_{86}N_4O_{19}$: 1442.0.

Sulforhodamine (Lissamine Red) taxoid ***5d***

A solution of compound **4** (19 mg, 0.021 mmol) in 1:1 dioxane:saturated aqueous sodium bicarbonate (1.5 ml) at room temperature under argon was treated with 6-chlorosulfonyl-2-sulfoxytetraethyl-rhodamine (Lissamine Rhodamine B chloride) (15 mg, 0.026 mmol, 1.25 eq). After 2 h, the mixture was diluted with aqueous sodium chloride (5 ml) and extracted (10 × 10 ml) with ethyl acetate. The combined organic layer was evaporated and the residue purified by HPLC (a gradient of 80 % 20 mM ammonium acetate in methanol to 100 % methanol over 30 min) to give compound **5b** as a deep purple film (22 mg, 75 %): mp > 300 °C; R_f = 0.54 (silica, 1 % AcOH and 10 % MeOH in methylene chloride); IR (thin film) ν_{max} 1064, 1156, 1550, 1601, 1720, 1756, 2986, 3690 cm^{-1}; ^{1}H NMR (500 MHz, CD_3OD) δ, 0.97 (s, 3 H, 16-H), 1.01 (s, 3 H, 17-H), 1.16 (m, 12 H, CH_3CH_2N), 1.61 (s, 3 H, 19-H), 1.61–1.64 (m, 1 H, 6β-H), 1.74 (s, 3 H, 18-H), 1.81–1.85 (m, 1 H, 14-H), 2.04 (s, 3 H, 10-OAc-H), 2.03–2.12 (m, 1 H, 14-H), 2.21 (s, 3 H, 4-OAc-H), 2.33–2.47 (band, 3 H, CH_2, 6α-H), 3.10–3.18 (m, 2 H, CH_2), 3.53 (br t, 8 H, *J* = 7, CH_2N), 3.76 (d, *J* = 7, 1 H, 3-H), 4.06 (dd, *J* = 8.5, 12, 2 H, 20-H, AB), 4.60 (d, *J* = 5, 1 H, 2′-H), 4.85 (d, *J* = 9, 1 H, 5-H), 5.42–5.5 (band, 3 H, 2-H, 3′-H, 7-H), 6.01 (br t, *J* = 9, 1 H, 13-H), 6.09 (s, 1 H, 10-H), 6.80 (brs, 2 H, Ar-H), 6.84 (m, 2 H, Ar-H), 6.97 (m, 2 H, Ar-H), 7.17 (br t, *J* = 9, 1 H, NH), 7.22–7.43 (band, 12 H, ArH), 7.53 (m, 1 H, Ar-H), 7.72 (d, *J* = 8, 1 H, Ar-H), 8.01 (d, *J* = 9, 1 H, Ar-H), 8.03 (dd, *J* = 2, 7, 1 H, Ar-H), 8.54 (br s, 1 H, Ar-H); ^{13}C NMR

(125 MHz, CD_3OD) δ 11.6, 12.9, 14.8, 21.0, 22.8, 23.6, 26.7, 34.2, 35.4, 36.2, 39.0, 44.6, 46.8, 47.2, 56.9, 57.8, 72.3, 73.4, 74.9, 76.0, 77.1, 77.4, 78.5, 82.1, 85.3, 97.0, 115.0, 115.1, 116.0, 116.1, 127.5, 128.5, 129.0, 129.4, 129.6, 129.8, 131.2, 131.3, 132.0, 132.9, 133.1, 133.2, 133.9, 133.9, 134.4, 135.5, 135.6, 140.0, 142.5, 144.0, 147.3, 157.2, 157.3, 158.0, 159.6, 167.6, 170.6, 171.0, 171.3, 172.1, 174.3, 204.0; positive electrospray *m/e* found: 1487.0 ($M + H^+$); calc'd for $C_{77}H_{85}N_4S_2O_{21}$: 1487.0.

Solubility measurements

The taxoid (1 mg) was placed in a 2-ml Eppendorf tube and suspended in deionized water (1 ml) with the aid of sonication for 5 min. The tubes were spun at 14 000 rpm for 1 min in a microcentrifuge to settle particulate matter. The solution was then carefully removed and filtered through a syringe filter (Dupont, 0.45 μm PTFE). Solubility was determined by measuring the UV absorbance of an aliquot of the aqueous solution at 254 nm and comparing to a standard curve produced by standard dilution of a 1 mM solution of the taxoid in methanol.

Partition coefficient

After the solubility of the taxoid was measured as above, the solution was replaced in the original Eppendorf tube, nonanol (1 ml) was added, and the mixture shaken vigorously for 5 min. The tubes were centrifuged to settle any particulate matter and the layers were separated. Partition coefficients were determined by comparing the UV absorbance of the layers at 254 nm.

Stability

The stability of the taxoids was measured by thin layer chromatography of a 1 mM solution in ethanol. The solutions were kept at ambient temperature under air and the purity checked each day. The experiment was discontinued after two weeks when no significant degradation was detected. The stability was confirmed by examining the ^1H NMR spectra of each compound at the end of the experiment.

Biology

Cytotoxicity measurements

Cells (ATTC HeLa and CHO, 1250 per well) were plated on 96-well plates in RPMI media with fetal calf serum (FCS) (245 μl per well) and grown to ~50 % confluence (24 h). The taxoids were diluted in ethanol and added as 5 μl aliquots directly to the wells to give final concentrations ranging from 1×10^{-4} to 1×10^{-10} M for each compound. The experimental controls were ethanol (5 μl) as the negative cytotoxicity control and sodium dodecylsulfate (1×10^{-3} M final concentration) as the positive cytotoxicity control. The growth inhibition was determined using the standard XTT assay [41].

Tubulin polymerization assays

Microtubules were prepared from the brains of 1–3 day old baby chicks (Hall Bros. Hatchery, Norwich, CT) by the standard double polymerization–depolymerization cycling in PM buffer [39,47]. On the day of a polymerization experiment, the microtubules and overlay buffer were thawed quickly. As the buffer thawed, the pellet was resuspended in the overlay buffer by gentle trituration with a Pasteur pipet. A final round of assembly at 37 °C followed by disassembly and clarification at 4 °C was performed to select for assembly competent protein after the period of storage. The resulting solution of 3× assembled microtubules (tubulin plus MAPs) was used in the assembly experiments reported herein. Polymerization assays were carried out on three-cycled tubulin in PIPES buffer (100 mM, pH 6.9) containing GTP (2 mM), $MgSO_4$ (5 mM), and EGTA (1 mM) [41]. The protein was not further purified and thus retained the MAPs. The tubulin solution was treated with taxoid (10 μM) and allowed to polymerize at 37 °C while the optical density was monitored at 340 nm.

Microscopy

Human foreskin fibroblasts were treated at 37 °C with taxoids at 20 μM, a concentration that is equimolar with that of cellular tubulin (E.D. Salmon, personal communication). After 1 h or 24 h, cells were observed with a Zeiss Axiophot microscope using differential interference contrast and fluorescence optics via a 40× 1.3 N.A. objective or a 100× 1.4 N.A. objective. Color micrographs were recorded on Kodak Ektachrome exposed at an ASA of 400 and developed commercially. Confocal microscope images were generated by a BioRad MRC 1000 operating on a Nikon microscope with a 63× 1.4 N.A. objective and captured electronically and stored on magnetic media. Composite color figures were produced either from stored electronic images or by scanning color photographs and manipulating the resulting files with Adobe Photoshop. Cells were fixed first in 3.7 % formaldehyde in PBS (phosphate buffered saline, pH 7.0) for 15 min at room temperature and then in 100 % methanol at −20 for 10 min. Following the methanol fixation and permeablization step, the cells were rehydrated in PBS and then stained with a monoclonal antibody to α tubulin (Sigma Chemical Co.) followed by the appropriate fluorescent secondary antibody (Kirkegaard and Perry, Inc.). Both the primary and secondary antibodies were used at the dilutions recommended by the respective suppliers of the antibodies. For images of living cells, the fixation and permeabilization steps were omitted.

Acknowledgements

We thank Klaus Hahn and Dai Vo for their assistance with cytotoxicity measurements. R.K.G. thanks Anne-Marie Yvon and Jennifer Waters for helpful discussions and suggestions. The work was supported financially by the George Hewitt Foundation for Medical Research (RKG), NSF grant MCB 93-16540 (R.D.S.) and the NIH (K.C.N.). D. Huang and G. Siuzdak are thanked for NMR and mass spectroscopic assistance, respectively.

References

1. Nicolaou, K.C., Dai, W.M. & Guy, R.K. (1994). Chemistry and biology of taxol. *Angew. Chem. Int. Ed.* **106**, 15–44.
2. Kingston, D.G., Molinero, A.A. & Rimoldi, J.M. (1993). The taxane diterpenoids. *Fortschr. Chem. Organ. Nature* **61**, 1–206.
3. Wani, M.C., Taylor, H.L., Wall, M.E., Coggon, P. & McPhail, A.T. (1971). Plant antitumor agents. VI. The isolation and structure of taxol, a novel antileukemic and antitumor agent from *Taxus brevifolia*. *J. Am. Chem. Soc.* **93**, 2325–2327.
4. Wall, M.E. & Wani, M.C. (1995). Paclitaxel: from discovery to clinic. *ACS Symp. Ser.* **583** (Taxane Anticancer Agents), 18–30.
5. Schiff, P.B., Fant, J. & Horwitz, S.B. (1979). Promotion of microtubule assembly *in vitro* by taxol. *Nature* **277**, 665–667.
6. Manfredi, J.J. & Horwitz, S.B. (1984). Taxol: an antimitotic agent with a new mechanism of action. *Pharmacol. Ther.* **25**, 83–125.
7. Hortobagyi, G.N., Holmes, F.A., Theriault, R.L. & Buzdar, A.U. (1994). Use of taxol (paclitaxel) in breast cancer. *Oncology* **51**, 29–32.
8. Gore, M.E., *et al.*, & Thompson, J.M. (1995). Paclitaxel (taxol) in relapsed and refractory ovarian cancer: the UK and Eire experience. *Br. J. Cancer* **72**, 1016–1019.
9. Rowinsky, E.K. (1994). Update on the antitumor activity of paclitaxel in clinical trials. *Ann. Pharmacother.* **28**, 18–22.
10. Wuthers, J.C., Mitchison, T.J., Reider, C.L. & Salmon, E.D. (1996). The kinetochore microtubule minus-end disassembly associated with poleward flux produces a force that can do work. *Mol. Biol. Cell* 7, 1547–1558.
11. Ludeña, R.F., Banerjee, A. & Khan, I.A. (1992). Tubulin structure and biochemistry. *Curr. Opin. Cell Biol.* **4**, 53–57.
12. Nogales, E., Wolf, S.G., Khan, I.A., Luduena, R.F. & Downing, K.H. (1995). Structure of tubulin at 6.5 Å and location of the taxol-binding site. *Nature* **375**, 424–427.
13. Purich, D.L. & Angelastro, J.M. (1994). Microtubule dynamics: bioenergetics and control. *Adv. Enz.* **69**, 121–154.
14. Cassimeris, L. (1993). Regulation of microtubule dynamic instability. *Cell Motil. Cytoskeleton.* **26**, 275–281.
15. Inoué, S. & Salmon, E.D. (1995). Force generation by microtubule assembly/disassembly in mitosis and related movements. *Mol. Biol. Cell* **6**, 1619–1640.
16. Wilson, L. & Jordan, M.A. (1995). Microtubule dynamics: taking aim at a moving target. *Chemistry & Biology* **2**, 569–573.
17. Derry, W.B., Wilson, L. & Jordan, M.A. (1995). Substoichiometric binding of taxol suppresses microtubule dynamics. *Biochemistry* **34**, 2203–2211.
18. Long, B.H. & Fairchild, C.R. (1994). Paclitaxel inhibits progression of mitotic cells to G1 phase by interference with spindle formation without affecting other microtubule functions during anaphase and telephase. *Cancer Res.* **54**, 4355–4361.

19. Lopes, N.M., Adams, E.G., Pitts, T.W. & Bhuyan, B.K. (1993). Cell kill kinetics and cell cycle effects of taxol on human and hamster ovarian cell lines. *Cancer Chemother. Pharmacol.* **32**, 235–242.
20. Roberts, J.R., Rowinsky, E.K., Donehower, R.C., Robertson, J. & Allison, D.C. (1989). Demonstration of the cell cycle positions of taxol-induced 'asters' and 'bundles' by sequential measurements of tubulin immunofluorescence, DNA content, and autoradiographic labeling of taxol-sensitive and -resistant cells. *J. Histochem. Cytochem.* **37**, 1659–1665.
21. Keller, H.U. & Zimmermann, A. (1986). Shape changes and chemokinesis of Walker 256 carcinosarcoma cells in response to colchicine, vinblastine, nocodazole and taxol. *Invasion Metastasis* **6**, 33–43.
22. Cameron, M.R., Caudle, M.R., Sullivan, W.R., Jr., Peluso, J.J. & Wimalasena, J. (1995). The steroidogenic and morphological effects of paclitaxel on cultured ovarian cancer cells. *Oncol. Res.* **7**, 145–156.
23. Thuret-Carnahan, J., Bossu, J.L., Feltz, A., Langley, K. & Aunis, D. (1985). Effect of taxol on secretory cells: functional, morphological, and electrophysiological correlates. *J. Cell Biol.* **100**, 1863–1874.
24. Roytta, M., Laine, K.M. & Harkonen, P. (1987). Morphological studies on the effect of taxol on cultured human prostatic cancer cells. *Prostate* **11**, 95–106.
25. Masurovsky, E.B., Peterson, E.R., Crain, S.M. & Horwitz, S.B. (1983). Morphological alterations in dorsal root ganglion neurons and supporting cells of organotypic mouse spinal cord ganglion cultures exposed to taxol. *Neuroscience* **10**, 491–509.
26. Hunt, C. & Stebgings, H. (1994). Taxol causes rapid gross structural rearrangement of a native microtubule bundle. *Cell Biochem. Funct.* **12**, 191–200.
27. Roy, C., Chaly, N. & Brown, D.L. (1988). Taxol-induced reorganization of the microtubule system in murine splenic lymphocytes inhibits response to allogeneic cells but not to concanavalin A. *Biochem. Cell Biol.* **66**, 389–395.
28. Green, K.J. & Goldman, R.D. (1983). The effects of taxol on cytoskeletal components in cultured fibroblasts and epithelial cells. *Cell Motil. Cytoskeleton* **3**, 283–305.
29. Kingston, D.G. (1991). The chemistry of taxol. *Pharmacol. Ther.* **52**, 1–34.
30. Sengupta, S., Boge, T.C., Georg, G.I. & Himes, R.H. (1995). Interaction of a fluorescent paclitaxel analog with tubulin. *Biochemistry* **34**, 11889–11894.
31. Souto, A.A., *et al.*, & Amat-Guerri, F. (1996). New fluorescent water-soluble taxol derivatives. *Angew. Chem. Int. Ed. Engl.* **34**, 2710–2712.
32. Dubois, J., *et al.*, & Wright, M. (1995). Fluorescent and biotinylated analogues of docetaxel: synthesis and biological evaluation. *Bioorg. Med. Chem. Lett.* **3**, 1357–1368.
33. Kingston, D.G.I. (1994). Taxol: the chemistry and structure–activity relationships of a novel anticancer agent. *Trends Biotechnol.* **12**, 222–227.
34. Chen, S.-H., *et al.*, & Farina, V. (1994). Taxol structure–activity relationships: synthesis and biological evaluation of taxol analogs modified at C-7. *Bioorg. Med. Chem. Lett.* **4**, 2223–2228.
35. Grover, S., *et al.*, & Hamel, E. (1995). Differential effects of paclitaxel (taxol) analogs modified at positions C-2, C-7, and C-3′ on tubulin polymerization and polymer stabilization: identification of a hyperactive paclitaxel derivative. *Biochem.* **34**, 3927–3934.
36. Takoudju, M., Wright, M., Chenu, J., Gueritte-Voegelein, F. & Guenard, D. (1988). Interaction of 7-acetyltaxol with different tubulin assemblies. *FEBS Lett.* **234**, 177–180.
37. Deutsch, H.M., *et al.*, & Zalkow, L.H. (1989). Synthesis of congeners and prodrugs. 3. Water-soluble prodrugs of taxol with potent antitumor activity. *J. Med. Chem.* **32**, 788–792.
38. Gaskin, F. (1982). Techniques for the study of microtubule assembly *in vitro*. *Methods Enzymol.* **85**, 433–440.
39. Sloboda, R.D. (1992). Methods for the purification and assay of microtubule-associated proteins. In *The Cytoskeleton: A Practical Approach*. (Carraway, K.L. & Carraway, A.C., eds), pp. 167–196, Oxford University Press, NY, USA.
40. Maccioni, R.B. & Cambiazo, V. (1995). Role of microtubule associated proteins in the control of microtubule assembly. *Physiol. Revs.* **75**, 835–864.
41. Scudiero, D.A., *et al.*, & Boyd, M.R. (1988). Evaluation of a soluble tetrazolium/formazan assay for cell growth and drug sensitivity in culture using human and other tumor cell lines. *Cancer Res.* **48**, 4827–4833.
42. Paloma, L.G., Guy, R.K., Wrasidlo, W. & Nicolaou, K.C. (1994). Conformation study of a water-soluble derivative of taxol in water by 2D-NMR spectroscopy. *Chemistry & Biology* **1**, 107–112.
43. Schatten, G., Schatten, H., Bestor, T.H. & Balczon, R. (1982). Taxol inhibits the nuclear movements during fertilization and induces asters in unfertilized sea urchin eggs. *J. Cell Biol.* **94**, 455–465.
44. Arbuck, S.G., Canetta, R., Onetto, N. & Christian, M.C. (1993). Current dosage and schedule issues in the development of paclitaxel (Taxol). *Semin. Oncol.* **20**, 31–39.
45. Wang, Y., Loomis, P.A., Zinkowski, R.P. & Binder, L.I. (1993). A novel tau transcript in cultured human neuroblastoma cells expressing nuclear tau. *J. Cell Biol.* **121**, 257–267.
46. Loomis, P.A., Howard, T.H., Castleberry, R.P. & Binder, L.I. (1990). Identification of nuclear tau isoforms in human neuroblastoma cells. *Proc. Natl. Acad. Sci. USA* **87**, 8422–8426.
47. Gaskin, F. (1981). *In vitro* microtubule assembly regulation by divalent cations and nucleotides. *Biochemistry* **20**, 1318–1322.